

Enhanced Sensing and Nondegraded Thermal Noise Performance Based on \mathcal{PT} -Symmetric Electronic Circuits with a Sixth-Order Exceptional Point

Zhicheng Xiao¹, Huanan Li², Tsampikos Kottos³, and Andrea Alù^{1,2,*}

¹*Department of Electrical and Computer Engineering, The University of Texas at Austin, Austin, Texas 78712, USA*

²*Advanced Science Research Center, City University of New York, New York, New York 10031, USA*

³*Department of Physics, Wesleyan University, Middletown, Connecticut 06459, USA*



(Received 21 August 2019; published 18 November 2019)

An exceptional point (EP) is a non-Hermitian degeneracy where both eigenvalues and their corresponding eigenvectors coalesce. It was recently proposed and demonstrated that such spectral singularity can be utilized for enhanced sensing. Potential drawbacks of EP sensing include both fundamental resolution limit and noise effects that might mask the hypersensitive resonant splitting. Here, we address these issues by proposing a parity-time (\mathcal{PT})-symmetric sensing circuit bearing a sixth-order EP. By employing capacitive coupling channel as a sensing platform, we achieve an enhanced resonance shift proportional to the fourth-order root of the perturbation strength and maintain a high resolution for weak perturbation. Due to the low-pass feature of our circuit, thermal noise is mitigated down to a level comparable to its Hermitian counterpart, despite the presence of highly noisy gain and loss elements. Our EP sensing scheme offers combined enhanced sensitivity, improved resolution and nondegraded thermal noise performance, showing an exciting prospect for next-generation sensing technologies.

DOI: [10.1103/PhysRevLett.123.213901](https://doi.org/10.1103/PhysRevLett.123.213901)

Introduction.—Sensing is of fundamental importance in modern society, ranging from industrial process monitoring [1], biomedical sample ingredient analysis [2], to massive deployment of wireless sensor network for the internet of things [3,4]. Most sensors rely on resonant structures, analyzing spectrum shifts of a single resonance or spectrum splitting of two degenerate modes when a perturbation to be sensed occurs. Typical examples include nanoparticle detection with ultrahigh- Q photonic microresonators [5] and wireless sensors based on LC microwave resonators [6]. In general, the magnitude of frequency splitting is linearly proportional to the perturbation strength due to the Hermitian nature of these sensing systems [7,8]. The degenerate sensing point in these Hermitian systems is thus known as diabolic point (DP) [7,8].

Recent advances in the fields of non-Hermitian physics and \mathcal{PT} symmetry [9–26] have revealed that enhanced sensitivity can be achieved based on a new type of degenerate point, known as exceptional point (EP). At EPs, two or more eigenvalues and their corresponding eigenvectors coalesce, leading to a nondiagonalizable Hamiltonian that demonstrates an N th-order root law of eigenfrequency splitting when N degenerate eigenmodes are lifted by the perturbation [27]: $\Delta\omega \sim \epsilon^{1/N}$, where ϵ is the perturbation strength. The sensitivity is thus proportional to $(1/N)\epsilon^{1/N-1}$, which, for small perturbation, is much higher than the linear sensitivity $\Delta\omega \sim \epsilon$ of DPs, as evidenced by some experimental demonstrations [23,24].

Nonetheless, the possibility to implement EP sensing in various setups has triggered an ongoing debate over the last

year [28–32]. On the one hand, there is a fundamental resolution limit for EP sensing schemes based on purely lossy systems due to the presence of imaginary part of the eigenfrequencies [28]. This imaginary component leads to a broadening of the reflection or transmission spectrum and further sets a fundamental resolution limit on the sensitivity of the device [28]. This bound is analogous, in another context, to conventional optical diffraction limit, where the angular resolution is limited by resolvable distance between two overlapping Airy disk diffraction patterns from two adjacent point sources [33,34]. On the other hand, parity-time (\mathcal{PT})-symmetric sensing systems with balanced loss and gain units can potentially improve the resolution limit, given that proper readout design and perturbation strategy are deployed. However, these gain and loss elements unavoidably add noise into the system [29–31], imposing another fundamental bound on the sensitivity.

In this Letter, we endeavor to address these issues by proposing an enhanced sensing scheme based on a sixth-order EP supported by a \mathcal{PT} -symmetric electronic circuit [see Fig. 1(a)]. Instead of detecting the resonant frequency splitting, we detect the eigenfrequency shift by measuring the reflected signals at the lossy side of our circuit. First, we set our system to a static EP with zero eigenfrequency. When the system is perturbed from the ideal EP condition, a reflection dip emerges, and shifts away from the static point. The reflection dip exactly matches the purely real eigenfrequency of the system under perturbation and shows a resonant shift following a fourth-order root law with respect to the perturbation strength. These resonant shifts

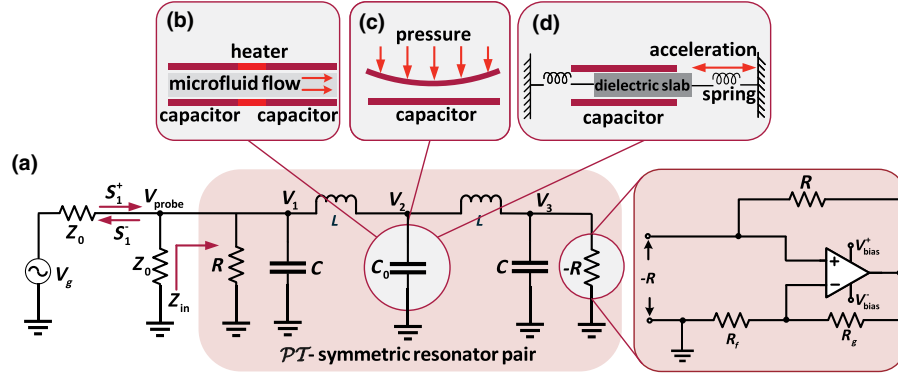


FIG. 1. Hypersensitive \mathcal{PT} -symmetric sensing circuit design and its possible application scenarios. (a) \mathcal{PT} -symmetric sensing circuit. The pink region consists of a pair of \mathcal{PT} -symmetric resonators. The negative impedance $-R$ is realized by an amplifier feedback circuit with noninverting configuration, where the gain coefficient is $1 + R_g/R_f$. The \mathcal{PT} -symmetric resonator pair is connected in shunt to a resistance Z_0 and then in series to a microwave generator with internal impedance Z_0 and voltage V_g . (b) Supersensitive microfluid flow sensor based on capacitive perturbation. The microfluid speed is sensed by measuring the temperature gradient created by the heater. (c) Supersensitive pressure sensor based on capacitive perturbation. A pressure sensitive membrane responds to external pressure and changes the effective capacitance of C_0 . (d) Supersensitive accelerometer based on capacitive perturbation. Acceleration is sensed by attaching a dielectric slab sandwiched within the capacitor plates and connected to two springs.

can be measured with high resolution, even for very weak perturbations. We further verify this claim through a comparative study of our EP sensing scheme with a DP sensing protocol supported by a similar circuit layout. As we show in the following, due to the low-pass feature of our sensing circuit, thermal noises are alleviated to an identical level as the corresponding DP sensing scheme.

Sixth-order exceptional point sensing system.—Our sensing scheme is based on a \mathcal{PT} -symmetric circuit supporting a sixth-order EP. The circuit design is shown in Fig. 1(a). In the pink-highlighted region, two resonators formed by a grounded capacitor C and a floating inductor L , are coupled with a grounded capacitor C_0 . A positive resistor R and a negative resistor $-R$ are connected in parallel with the left and right resonator, respectively.

To reveal the sensing mechanism in our scheme, we formulate the corresponding non-Hermitian Hamiltonian and study its eigenfrequency. Using Kirchhoff's laws, the dynamics of the voltages at various nodes of the isolated system follow these equations:

$$\begin{aligned} \dot{V}_1 + \gamma \dot{V}_1 + V_1 - V_2 &= 0, \\ \dot{V}_2 + 2\mu V_2 - \mu V_1 - \mu V_3 &= 0, \\ \dot{V}_3 - \gamma \dot{V}_3 - V_2 + V_3 &= 0, \end{aligned} \quad (1)$$

where $\dot{V}_n = dV_n/d\tau$, $\ddot{V}_n = d^2V_n/d\tau^2$, $n = 1, 2, 3$, $\tau = \omega_0 t$ is the normalized time, $\omega_0 = 1/\sqrt{LC}$ is the resonant frequency of the resonator, $\gamma = R^{-1}\sqrt{L/C}$ is the intrinsic loss or gain rate of the LC resonator, $\mu = C/C_0$ is the coupling coefficient between the two resonators. It is easy to show that Eq. (1) is invariant under a joint time-reversal ($\tau \rightarrow -\tau$) and parity operation ($V_1 \leftrightarrow V_3$; $V_2 \leftrightarrow V_2$), and therefore the system is \mathcal{PT} symmetric [13]. Constructing a

state vector for this six variable linear system $\Psi = [V_1 V_2 V_3 \dot{V}_1 \dot{V}_2 \dot{V}_3]^T$, we can recast Eq. (1) into the Schrödinger-type equation:

$$i \frac{d\Psi}{d\tau} = \begin{bmatrix} 0 & 0 & 0 & i & 0 & 0 \\ 0 & 0 & 0 & 0 & i & 0 \\ 0 & 0 & 0 & 0 & 0 & i \\ -i & i & 0 & -i\gamma & 0 & 0 \\ i\mu & -2i\mu & i\mu & 0 & 0 & 0 \\ 0 & i & -i & 0 & 0 & i\gamma \end{bmatrix} \Psi = H_{\text{eff}} \Psi, \quad (2)$$

where H_{eff} is the effective Hamiltonian describing the dynamics of our circuit. The eigenfrequencies are found through the associated characteristic equation $\text{Det}[H_{\text{eff}} - \mathbf{I}\omega] = 0$:

$$\omega^2[\omega^4 + (\gamma^2 - 2 - 2\mu)\omega^2 + 1 + 2\mu - 2\mu\gamma^2] = 0, \quad (3)$$

where \mathbf{I} is the six-dimensional unity matrix. Solving Eq. (3), we find the six eigenfrequencies:

$$\begin{aligned} \omega_{1,2} &= \pm \frac{1}{\sqrt{2}} \sqrt{2 + 2\mu - \gamma^2 + \sqrt{4\mu^2 - 4\gamma^2 + 4\mu\gamma^2 + \gamma^4}}, \\ \omega_{3,4} &= \pm \frac{1}{\sqrt{2}} \sqrt{2 + 2\mu - \gamma^2 - \sqrt{4\mu^2 - 4\gamma^2 + 4\mu\gamma^2 + \gamma^4}}, \\ \omega_{5,6} &= 0. \end{aligned} \quad (4)$$

There is always a pair of eigenfrequencies corresponding to the dc solution of the system, with the eigenstate $\Psi = [1 \ 1 \ 1 \ 0 \ 0 \ 0]^T$. Moreover, for an appropriate choice of γ , μ , all eigenfrequencies are degenerate at

$\omega_{\text{EP}} = 0$ with the same eigenvector $\Psi = [1 \ 1 \ 1 \ 0 \ 0 \ 0]^T$. This sixth-order EP occurs for the following:

$$\gamma_{\text{EP}} = (\sqrt{5} + 1)/2; \quad \mu_{\text{EP}} = (\sqrt{5} - 1)/4, \quad (5)$$

which are inherent properties of the circuit topology. The sixth-order EP is ideally suited for sensing applications if we consider a perturbation to the system. Here, we assume that the perturbation is applied to the coupling capacitor with $\mu = \mu_{\text{EP}}(1 + \epsilon)$, modeling the realistic scenario where the capacitor serves as a small sensing platform [see Figs. 1(b)–1(d)]. Since the sensed quantity is linearly proportional to the perturbation strength ϵ [35], the eigenfrequency response with respect to the sensed quantity is identical to the perturbation strength.

One-port scattering and readout setup.—We connect the \mathcal{PT} -symmetric resonator pair in shunt to a resistor Z_0 and in series with a microwave generator having same internal impedance Z_0 . This readout design ensures that the whole sensing network remains matched around the EP to the internal impedance of the generator, avoiding backward propagating waves reflected into the generator [38]. According to the readout circuit design in Fig. 1(a), the reflection coefficient can be expressed as

$$S_{11} = -Z_0(2Z_{\text{in}} + Z_0)^{-1}, \quad (6)$$

where Z_{in} is the input impedance of the \mathcal{PT} -symmetric resonator pair,

$$Z_{\text{in}} = \frac{i\gamma R[\omega^4 - i\gamma\omega^3 - (1 + 2\mu)\omega^2 + 2i\gamma\mu\omega + \mu]}{\omega[\omega^4 + (\gamma^2 - 2 - 2\mu)\omega^2 + 1 + 2\mu - 2\mu\gamma^2]}. \quad (7)$$

As expected, the denominator of Z_{in} corresponds to the characteristic equation of the \mathcal{PT} -symmetric system, which implies that the resonant dips of S_{11} directly correspond to the system eigenfrequency. The dependence of the resonant shift on a small perturbation ϵ can be found through a series expansion of the eigenfrequency around the EP:

$$\delta\omega_{\text{EP}} = \epsilon^{\frac{1}{4}} + \frac{\sqrt{5} - 1}{8}\epsilon^{\frac{3}{4}} + \mathcal{O}(\epsilon^{\frac{5}{4}}) + \dots, \quad (8)$$

where “ \mathcal{O} ” is an asymptotic notation.

We confirm our theoretical analysis by simulating the reflection amplitude for different perturbation strengths in Fig. 2(a). When the perturbation ϵ is 0, the system exactly operates at a sixth-order EP with eigenfrequency $\omega_{\text{EP}} = 0$, leading to a resonant dip on the reflection spectrum. When the coupling coefficient μ increases, the whole sensing system deviates from the sixth-order EP. Consequently, another resonant dip arises and shifts to the right, clearly seen in Fig. 2(a). We extract these resonant dips $\delta\omega_{\text{EP}}$ and show them in Fig. 2(c). Our data indicate that the resonant

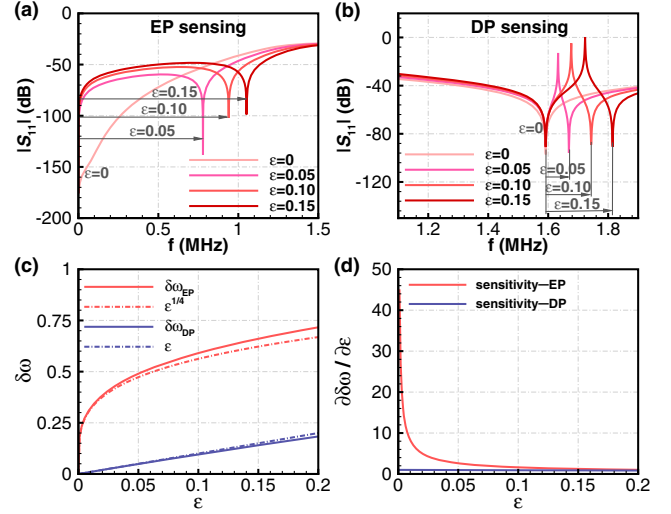


FIG. 2. Amplitude of reflection coefficient, eigenfrequency shift, and sensitivity at EP and DP. (a) Amplitude of reflection coefficient with different perturbation strength for EP sensing system. (b) Amplitude of reflection coefficient for DP sensing system. (c) Eigenfrequency shift at EP and DP, dashed lines represent the corresponding series expansion truncated to the first order. (d) Sensitivity at EP and DP versus the perturbation. The components are chosen as follows: $L = 100 \mu\text{H}$, $C = 100 \text{ pF}$, $R = 618.03 \Omega$, $Z_0 = 50 \Omega$. For EP sensing system $C_0 = 323.6 \text{ pF}$; for DP system $C_0 = 0.1 \mu\text{F}$. The above ADS simulation results confirmed our theory (see the Supplemental Material for circuit schematic [35]).

frequency shift is proportional to the fourth-order root of the perturbation strength, as expected.

To prove that the higher-order EP in our electronic circuit offers enhanced sensitivity compared to conventional sensors, we study an analogous Hermitian sensing circuit supporting a DP. Referring to Fig. 1(a), the Hermitian counterpart of our circuit layout can be realized by removing both the loss element R and the gain element $-R$. The Hermitian system operates at a second order DP as the coupling coefficient μ goes to 0. In Fig. 2(b), we report the reflection amplitude associated with this circuit for various perturbation strengths. The corresponding eigenfrequency shift $\delta\omega_{\text{DP}}$ is also shown in Fig. 2(c). Both curves confirm that the resonant frequency shift is linearly proportional to the perturbation strength for DP sensing. We compare the sensitivity of our EP and DP sensing schemes in Fig. 2(d), showing that the higher-order EP sensing scheme indeed provides enhanced sensitivity.

A perturbation on the resistor, inductor, or capacitor in the resonator, in principle, can result in frequency shift or splitting. However, these perturbation schemes inevitably bring in complex eigenfrequencies, which broaden the line shape and create a wide unresolvable region [28], as shown in previous EP sensor demonstrations [23,24]. Our design is devoid of these complex eigenfrequencies and therefore dramatically improves the sensing resolution, especially for

small perturbations. Our assessments are further confirmed in the Supplemental Material [35]. In practice, sophisticated techniques should be involved to maintain a good match between the gain and loss parameter [32].

Mitigating thermal noise.— \mathcal{PT} -symmetric circuitry relies on additional gain and loss elements, prone to add noise to the system. This issue has raised a degree of skepticism from the community concerning the effectiveness of EP sensing protocols [29–31]. There are shot noise, flicker noise, and thermal noise in an electronic circuit. Since the shot noise mainly exists in circuits with tunneling diode or vacuum tube, and flicker noise can be significantly reduced below the level of thermal noise by choosing wire-wound resistors [39–42], we aim for analyzing thermal noise in this Letter. In the following, we will show how thermal noise is alleviated in our sensing scheme.

Thermal noise in an electronic circuit is characterized by the power spectral density (PSD) which reads: $S_i(f) = 4k_B T |H_i(f)|^2 R_i$ [39–42], where k_B is the Boltzmann constant, T is the temperature, R_i is the resistance of the noise source, and $H_i(f)$ is the transfer function. The latter defines the voltage ratio between the probing point [see Fig. 1(a)] and the noise source. We first look into the PSD associated with the internal impedance of the generator. Assuming that there is an equivalent voltage noise source in series with the internal impedance Z_0 , we find that the transfer function takes the form $H_1(f) = Z_{in}/(2Z_{in} + Z_0)$. Since the resistor Z_0 is in shunt with the internal impedance Z_0 , the transfer function is $H_2(f) = H_1(f)$, leading to an identical PSD to the internal impedance Z_0 . For the loss element R , the transfer function is $H_3(f) = Z_{in}Z_0/(Z_{in}Z_0 + RZ_0 + 2RZ_{in})^{-1}$. The noise from the negative impedance $-R$ is more complicated to assess because it depends on the specific circuit design implementing the negative impedance. Here, we assume to use an amplifier circuit with noninverting feedback configuration. The feedback impedance is thus set to R , which indicates that the noise PSD is proportional to R . The thermal noise PSD from each noise source is shown in Fig. 3(a), which indicates that the noise PSD from the gain and loss elements are negligible compared to those stemming from the two Z_0 elements. We conclude therefore that the total thermal noise PSD in the \mathcal{PT} -symmetric sensing system and its corresponding Hermitian system are almost identical. Figures 3(c) and 3(d) show the theoretical and numerical thermal noise PSD provided by ADS software, which are in excellent agreement with each other.

Integrated noise power and signal to noise ratio (SNR) are important metrics of thermal noise as well. In a circuit with N independent noise sources, the total noise power can be expressed as

$$P_{\text{noise}} = \overline{V_{\text{noise}}^2} = \sum_{i=1}^N \int_0^{\infty} S_i(f) df, \quad (9)$$

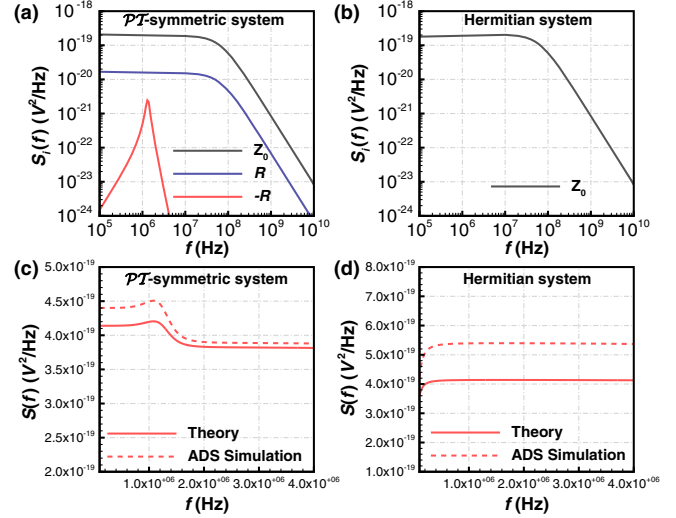


FIG. 3. Thermal noise power spectral density. The circuit parameters are identical to Fig. 2. (a) Thermal noise power spectral density from the impedance Z_0 , from the resistor R , and from the gain element $-R$, respectively, in the \mathcal{PT} -symmetric system. (b) Thermal noise power spectral density from the impedance Z_0 in the corresponding Hermitian system. (c) Total thermal noise power spectral density in the \mathcal{PT} symmetric system, dashed line indicates the ADS simulation results. (d) Total thermal noise power spectral density in the corresponding Hermitian system, the dashed line indicates ADS simulation results (see the Supplemental Material for circuit schematic [35]).

where V_{noise} is the noise voltage. Since the noise power from the resistor R and $-R$ are negligible compared with the impedance Z_0 , we only consider the noise power from the internal impedance Z_0 and shunt resistor Z_0 . Substituting the transfer function into Eq. (9), the approximate thermal noise power from each Z_0 takes the form: $k_B T/2C$, indicating that the noise power is independent of the impedance value Z_0 , the inductance L , and the coupling capacitance C_0 . Therefore, the noise power in our \mathcal{PT} -symmetric sensing network and the Hermitian counterpart are:

$$P_{\text{noise}}^{\mathcal{PT}} \approx P_{\text{noise}}^{\text{Hermitian}} \approx k_B T/C, \quad (10)$$

an expression identical to the integrated noise of a low pass RC filter [42]. This result indicates that the integrated thermal noise of the \mathcal{PT} -symmetric and Hermitian sensing systems are identical due to the low pass feature of our design. When the system is perturbed, the total noise power slightly changes, but this variation is negligible. At EP or DP, the resonator pair is essentially open, which results in $V_g/2$ signal voltage at the probing point, where V_g is the voltage of the generator. Therefore, the SNR at EP or DP is

$$\text{SNR}^{\text{EP}} \approx \text{SNR}^{\text{DP}} = \frac{(V_g/2)^2}{P_{\text{noise}}} \approx \frac{CV_g^2}{4k_B T}. \quad (11)$$

Finally, we study the influence of thermal noise on measurement results. The probing voltage V_{probe} and the

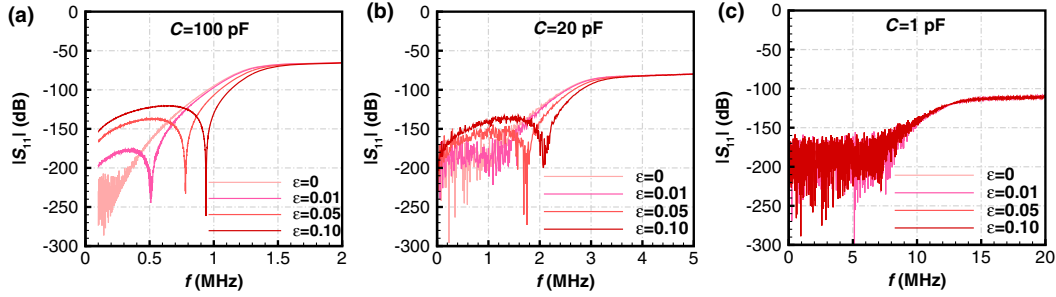


FIG. 4. Simulation of measurement results under the influence of thermal noise. The circuit parameters are identical to Fig. 2, except for the capacitor C in the resonator. The temperature T is 300 K and the voltage of the generator V_g is 1 V. (a) Amplitude of reflection coefficient, with $C = 100$ pF. (b) Amplitude of reflection coefficient, with $C = 20$ pF. (c) Amplitude of reflection coefficient, with $C = 1$ pF.

reflection coefficient S_{11} in our sensing network has an intuitive relation: $S_{11} = 2(V_{\text{probe}} + V_{\text{noise}})/V_g - 1$. Therefore, the deviation of the reflection coefficient is

$$D[S_{11}]^{\mathcal{PT}} \approx D[S_{11}]^{\text{Hermitian}} = \frac{4}{V_g^2} \frac{V_{\text{noise}}^2}{V_g^2} \approx \frac{4k_B T}{C V_g^2}, \quad (12)$$

where “ D ” indicates the deviation. Equations (10)–(12) prove that our EP sensing system shares the same thermal noise performance compared with the corresponding DP sensing scheme. Figure 4 shows the simulation of measurements under the influence of thermal noise. Figure 4(a) corresponds to the sensing circuit we designed in this work, where thermal noise has little influence on the measurement results, confirming that thermal noise in our EP sensing system is fully manageable by choosing a proper working capacitance value in the resonator. Figure 4(b) shows a marginal design, for which the measurement results can still be recorded. Figure 4(c) demonstrates a failed design, where the signal is fully buried by thermal noise and no sensing can be performed.

Conclusions.—In this Letter, we have put forward a sensing circuit based on a sixth-order EP, showing an enhanced resonant shift proportional to the fourth-order root of the perturbation strength. Due to the balanced loss and gain configuration and our perturbation scheme, the resolution is also improved. Our \mathcal{PT} -symmetric system not only serves as a sensing platform, but also filters out high-frequency thermal noise, leading to a nearly identical thermal noise level compared to the corresponding Hermitian DP sensing scheme. Considering the combined high-sensitivity, improved resolution, and nondegraded thermal noise performance, we envision that accelerometers, pressure sensors, or microfluid flow speed sensors may be implemented following this scheme with unprecedented sensitivity, resolution, and excellent thermal noise performance, as sketched in Fig. 1.

Z. Xiao appreciates helpful discussions with group members Drs. S. Mann and M. Kang. T. Kottos acknowledges the hospitality of ASRC of CUNY (Photonics

Initiative) during his sabbatical stay when this work has been performed. This work has been supported by the DARPA NLM program, the Air Force Office of Scientific Research, the National Science Foundation and the Simons Foundation.

*aalu@gc.cuny.edu

- [1] L. Fortuna, S. Graziani, A. Rizzo, and M. G. Xibilia, *Soft Sensors for Monitoring and Control of Industrial Processes* (Springer, London, 2007).
- [2] K. Chughtai and R. M. A. Heeren, Mass spectrometric imaging for biomedical tissue analysis, *Chem. Rev.* **110**, 3237 (2010).
- [3] L. Mainetti, L. Patrono, and A. Vilei, Evolution of wireless sensor networks towards the Internet of Things: A survey, in *19th International Conference on Software, Telecommunications and Computer Networks* (IEEE, 2011).
- [4] N. Khalil, M. R. Abid, D. Benhaddou, and M. Gerndt, Wireless sensors networks for Internet of Things, in *IEEE Ninth International Conference on Intelligent Sensors, Sensor Networks and Information Processing (ISSNIP)* (IEEE, 2014).
- [5] J. Zhu, S. K. Ozdemir, Y.-F. Xiao, L. Li, L. He, D.-R. Chen, and L. Yang, On-chip single nanoparticle detection and sizing by mode splitting in an ultrahigh-Q microresonator, *Nat. Photonics* **4**, 46 (2010).
- [6] R. Nopper, R. Has, and L. Reindl, A wireless sensor readout system-circuit concept, simulation, and accuracy, *IEEE Trans. Instrum. Meas.* **60**, 2976 (2011).
- [7] M. V. Berry and M. Wilkinson, Diabolical points in the spectra of triangles, *Proc. R. Soc. A* **392**, 15 (1984).
- [8] D. Dubbers and H.-J. Stöckmann, *Diabolic Points, Geometric Phases, and Quantum Chaos* (Springer, Berlin, 2013).
- [9] C. M. Bender and S. Boettcher, Real Spectra in Non-Hermitian Hamiltonians Having PT Symmetry, *Phys. Rev. Lett.* **80**, 5243 (1998).
- [10] C. M. Bender, Making sense of non-Hermitian Hamiltonians, *Rep. Prog. Phys.* **70**, 947 (2007).
- [11] R. El-Ganainy, K. G. Makris, D. N. Christodoulides, and Z. H. Musslimani, Theory of coupled optical PT-symmetric structures, *Opt. Lett.* **32**, 2632 (2007).

- [12] C. E. Rüter, K. G. Makris, R. El-Ganainy, D. N. Christodoulides, M. Segev, and D. Kip, Observation of parity-time symmetry in optics, *Nat. Phys.* **6**, 192 (2010).
- [13] J. Schindler, A. Li, M. C. Zheng, F. M. Ellis, and T. Kottos, Experimental study of active LRC circuits with PT symmetries, *Phys. Rev. A* **84**, 040101 (2011).
- [14] Z. Lin, J. Schindler, F. M. Ellis, and T. Kottos, Experimental observation of the dual behavior of PT-symmetric scattering, *Phys. Rev. A* **85**, 050101 (2012).
- [15] J. Schindler, Z. Lin, J. M. Lee, H. Ramezani, F. M. Ellis, and T. Kottos, PT-symmetric electronics, *J. Phys. A* **45**, 444029 (2012).
- [16] L. Ge, Y. D. Chong, and A. D. Stone, Conservation relations and anisotropic transmission resonances in one-dimensional PT-symmetric photonic heterostructures, *Phys. Rev. A* **85**, 023802 (2012).
- [17] R. Fleury, D. Sounas, and A. Alù, An invisible acoustic sensor based on parity-time symmetry, *Nat. Commun.* **6**, 5905 (2015).
- [18] D. L. Sounas, R. Fleury, and A. Alù, Unidirectional Cloaking Based on Metasurfaces with Balanced Loss and Gain, *Phys. Rev. Applied* **4**, 014005 (2015).
- [19] J. Doppler, A. A. Mailybaev, J. Böhm, U. Kuhl, A. Girschik, F. Libisch, T. J. Milburn, P. Rabl, N. Moiseyev, and S. Rotter, Dynamically encircling an exceptional point for asymmetric mode switching, *Nature (London)* **537**, 76 (2016).
- [20] M.-A. Miri and A. Alù, Exceptional points in optics and photonics, *Science* **363**, eaar7709 (2019).
- [21] J. Wiersig, Enhancing the Sensitivity of Frequency and Energy Splitting Detection by Using Exceptional Points: Application to Microcavity Sensors for Single-Particle Detection, *Phys. Rev. Lett.* **112**, 203901 (2014).
- [22] J. Wiersig, Sensors operating at exceptional points: General theory, *Phys. Rev. A* **93**, 033809 (2016).
- [23] W. Chen, Ş. K. Özdemir, G. Zhao, J. Wiersig, and L. Yang, Exceptional points enhance sensing in an optical microcavity, *Nature (London)* **548**, 192 (2017).
- [24] H. Hodaei, A. U. Hassan, S. Wittek, H. Garcia-Gracia, R. El-Ganainy, D. N. Christodoulides, and M. Khajavikhan, Enhanced sensitivity at higher-order exceptional points, *Nature (London)* **548**, 187 (2017).
- [25] P.-Y. Chen, M. Sakhdari, M. Hajizadegan, Q. Cui, M. M.-C. Cheng, R. El-Ganainy, and A. Alù, Generalized parity-time symmetry condition for enhanced sensor telemetry, *Nat. Electron.* **1**, 297 (2018).
- [26] Z. Dong, Z. Li, F. Yang, C.-W. Qiu, and J. S. Ho, Sensitive readout of implantable microsensors using a wireless system locked to an exceptional point, *Nat. Electron.* **2**, 335 (2019).
- [27] K. Kato, *Perturbation Theory for Linear Operators* (Springer, Berlin, 1995).
- [28] W. Langbein, No exceptional precision of exceptional-point sensors, *Phys. Rev. A* **98**, 023805 (2018).
- [29] H.-K. Lau and A. A. Clerk, Fundamental limits and non-reciprocal approaches in non-Hermitian quantum sensing, *Nat. Commun.* **9**, 4320 (2018).
- [30] M. Zhang, W. Sweeney, C. W. Hsu, L. Yang, A. D. Stone, and L. Jiang, Quantum Noise Theory of Exceptional Point Sensors, *Phys. Rev. Lett.* **123**, 180501 (2019).
- [31] C. Chen, L. Jin, and R.-B. Liu, Sensitivity of parameter estimation near the exceptional point of a non-Hermitian system, *New J. Phys.* **21**, 083002 (2019).
- [32] N. A. Mortensen, P. A. D. Gonçalves, M. Khajavikhan, D. N. Christodoulides, C. Tserkezis, and C. Wolff, Fluctuations and noise-limited sensing near the exceptional point of parity-time-symmetric resonator systems, *Optica* **5**, 1342 (2018).
- [33] M. Born and E. Wolf, *Principles of Optics* (Cambridge University Press, Cambridge, England, 1997).
- [34] J. W. Goodman, *Introduction to Fourier Optics*, 3rd ed. (Roberts and Company Publishers, Englewood, Colorado, 2004).
- [35] See the Supplemental Material at <http://link.aps.org/supplemental/10.1103/PhysRevLett.123.213901> for analysis of the relation between the resonance shift and the sensed quantity, circuit layout in ADS, other sensing protocols based on perturbation over the capacitor and inductor in the resonator, and the influence of mismatch between the gain and loss parameter, which includes Refs. [25,36,37].
- [36] C. G. Malmberg and A. A. Maryott, Dielectric constant of water from 0 to 100 °C, *J. Res. NBS* **56**, 2641 (1956).
- [37] C. Li, Q. Tan, C. Xue, W. Zhang, Y. Li, and J. Xiong, A high-performance LC wireless passive pressure sensor fabricated using low-temperature co-fired ceramic (LTCC) technology, *Sensors* **14**, 23337 (2014).
- [38] D. M. Pozar, *Microwave Engineering*, 4th ed. (Wiley, New York, 2011).
- [39] H. Nyquist, Thermal agitation of electric charge in conductors, *Phys. Rev.* **32**, 110 (1928).
- [40] R. Kubo, The fluctuation-dissipation theorem, *Rep. Prog. Phys.* **29**, 255 (1966).
- [41] L. Reggiani and E. Alfinito, Fluctuation dissipation theorem and electrical noise revisited, *Fluctuation Noise Lett.* **18**, 1930001 (2019).
- [42] P. R. Gray, P. J. Hurst, S. H. Lewis, and R. G. Meyer, *Analysis and Design of Analog Integrated Circuits*, 5th ed. (Wiley, New York, 2009).